Supplement

Development and deployment of a mid-cost CO_2 sensor monitoring network to support atmospheric inverse modeling for quantifying urban CO_2 emissions in Paris

Jinghui Lian[1,2], Olivier Laurent[2], Mali Chariot[2], Luc Lienhardt[3], Michel Ramonet[2], Hervé Utard[1], Thomas Lauvaux[3], François-Marie Bréon[2], Grégoire Broquet[2], Karina Cucchi[1], Laurent Millair[1] and Philippe Ciais[2]

[1] Origins.earth, SUEZ Group, Tour CB21, 16 Place de l'Iris, 92040 Paris La Défense Cedex, France
[2] Laboratoire des Sciences du Climat et de l'Environnement (LSCE), IPSL, CEA-CNRS-UVSQ, Université Paris-Saclay, 91191 Gif sur Yvette Cedex, France
[3] Groupe de Spectrométrie Moléculaire et Atmosphérique (GSMA), Université de Reims-Champagne Ardenne, UMR CNRS 7331, Reims, France

Correspondence to: Jinghui Lian (jinghui.lian@suez.com) and Olivier Laurent (olivier.laurent@lsce.ipsl.fr)

This PDF file includes:

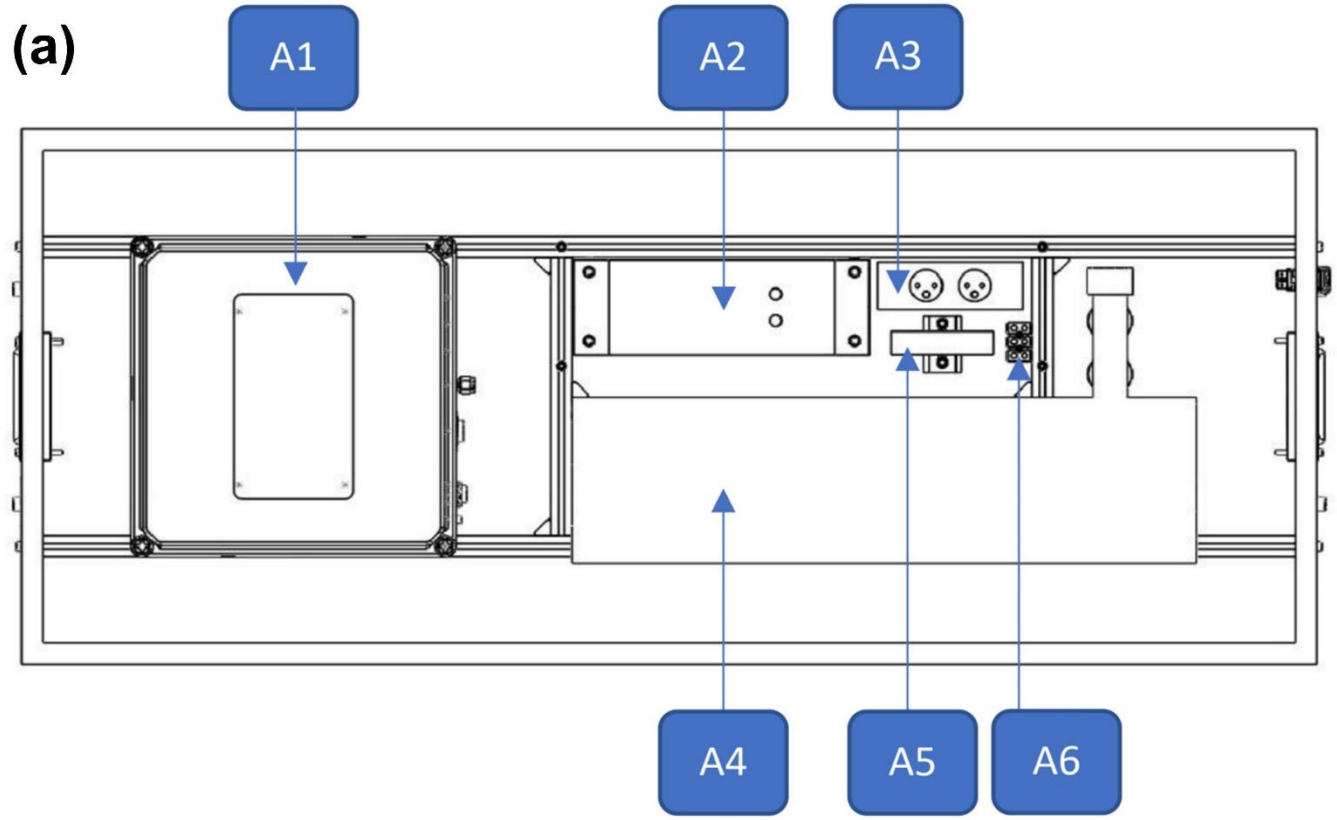

	Item	Description
A1	Slot for HPP sensor box	The HPP sensor box is installed by affixing it with four threaded screws
A2	Slot for flushing pump	Optional
A3	Power strips	Slot 1: HPP sensor box. Slot 2: flushing pump
A4	Slot for target gas container	5L tank
A5	12V power supply	For supplying the container fans
A6	Terminal block	The connection to the electrical network is done from here

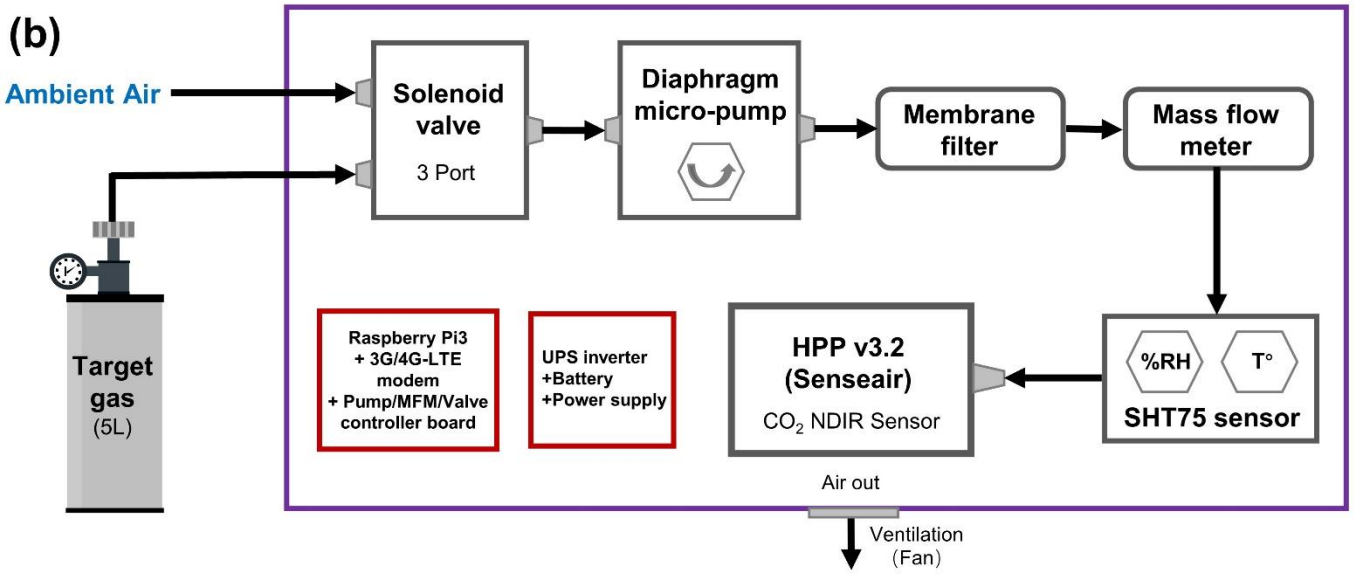

Figure S1. (a) Schematic of the integrated HPP CO_2 instrument for the field deployment, (b) Plumbing design of the airflow inside the integrated HPP sensor box, as shown in Figure 1b and located at A1 in (a). Figure (a) was made by © Eloneo (https://eloneo.fr/)

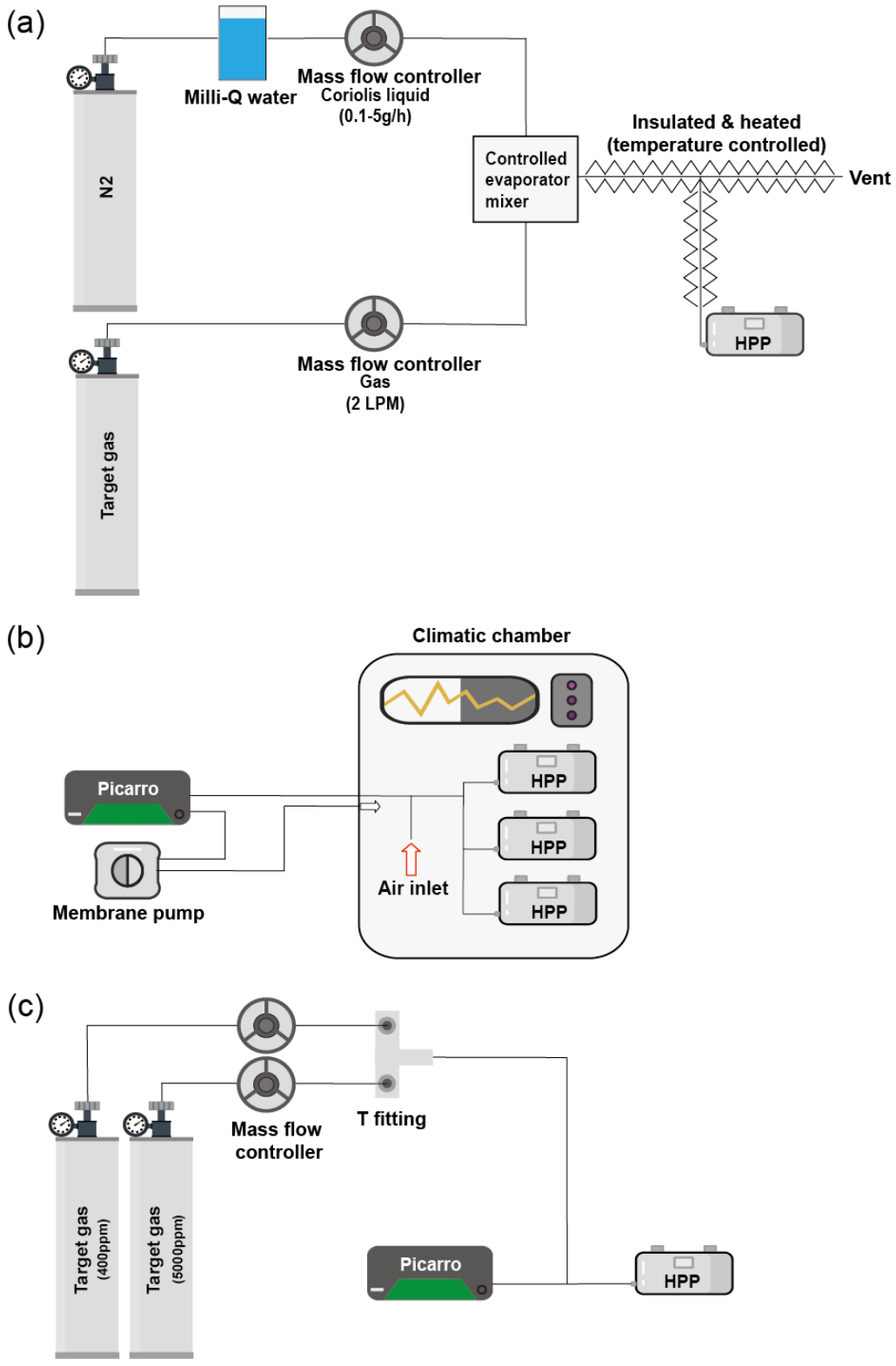

Figure S2. Schematic of the HPP laboratory (a) water vapor sensitivity test, (b) pressure and temperature sensitivity tests and (c) CO_2 sensitivity test for the calibration procedure. Note that all 8 HPP instruments have been subjected to these tests.

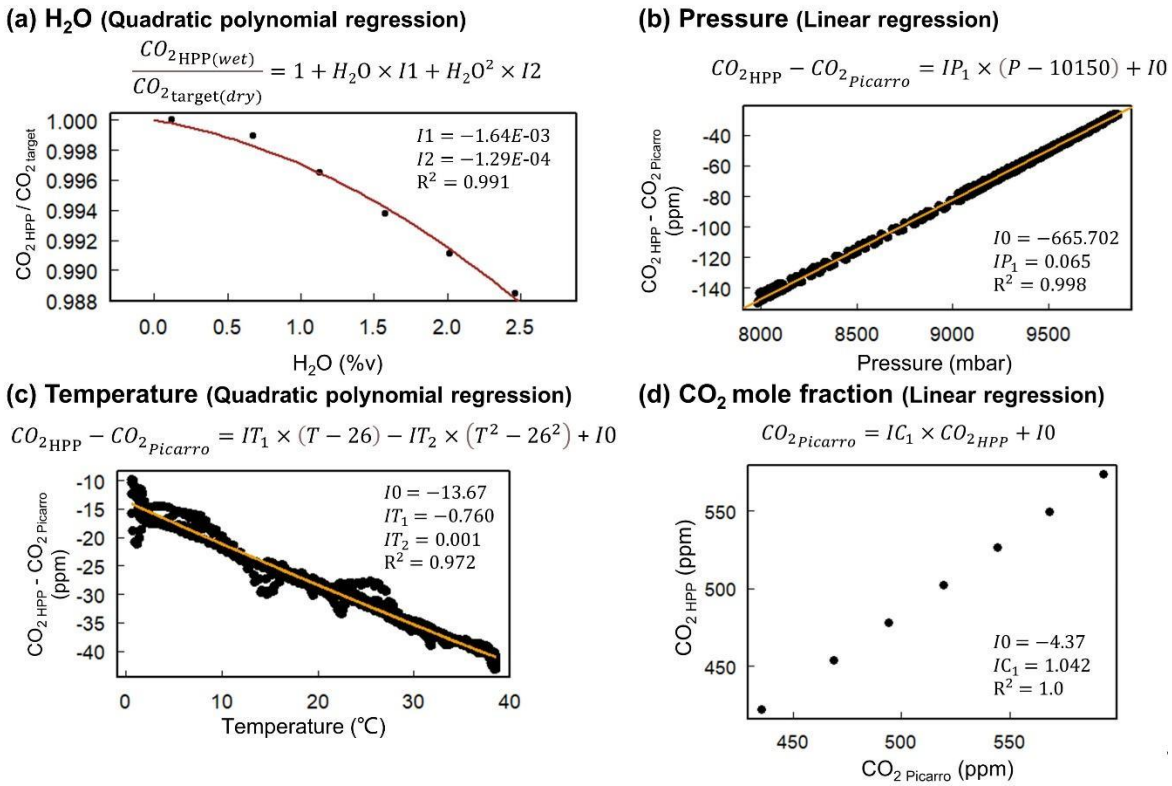

Figure S3. Relationships between the raw 1-minute averaged CO_2 mole fraction reported by one of the HPP sensors (HPP3) and variations in H_2O, T, p and CO_2 mole fraction in the sensitivity tests, respectively. The derived regression coefficients are used in the CO_2 calibration equation.

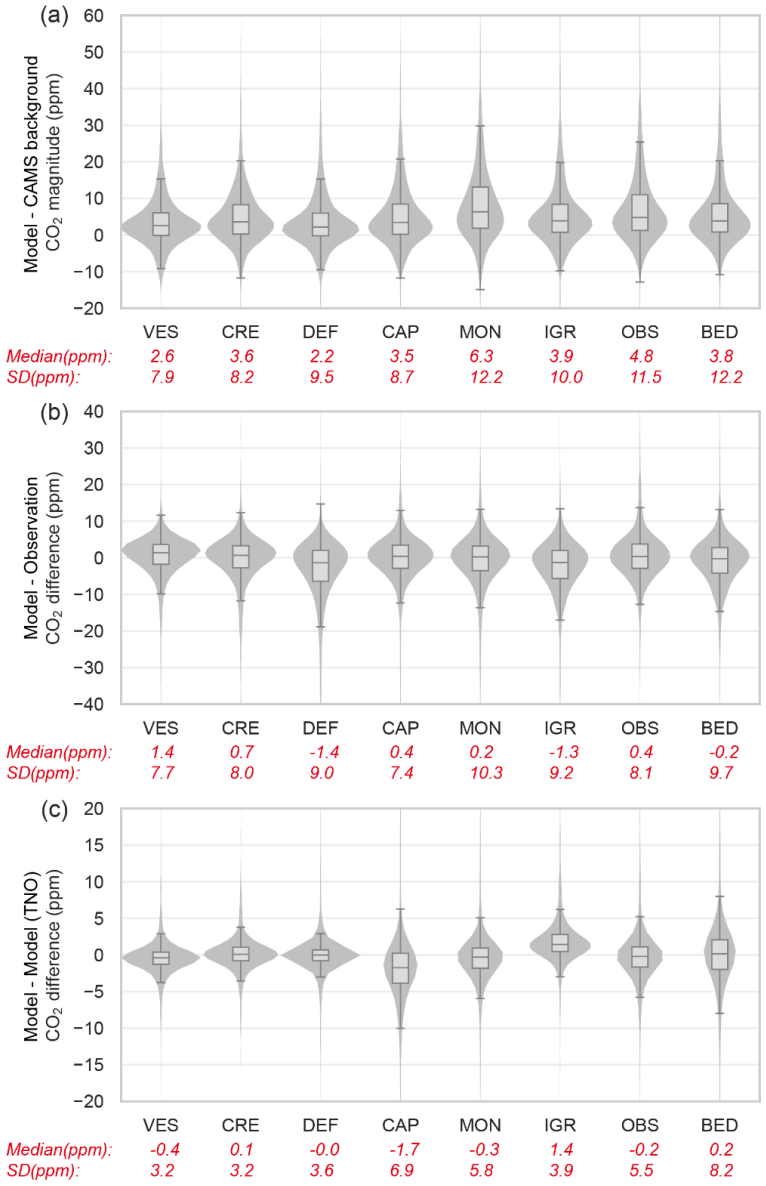

Figure S4. (a) Distribution of the local hourly afternoon (12-17 UTC) CO_2 signals at each HPP station from July 2020 to December 2022. This is computed by using the WRF-Chem simulated total CO_2 (fossil fuel, biogenic, and background sources) minus the background CO_2 mole fractions derived from the CAMS dataset. (b) Distribution of the differences in hourly afternoon CO_2 mole fraction between the WRF-Chem model and the observations at each HPP station from July 2020 to December 2022. (c) Distribution of the differences in simulated hourly afternoon CO_2 mole fraction, using Origins.earth (default) and TNO 1km inventory (Dellaert et al., 2019) as fossil fuel CO_2 emission inputs for the WRF-Chem model respectively. This model sensitivity test was carried out for the year 2018 (Lian et al., 2023). The midpoint, the box and the whiskers represent the 0.5 quantile, 0.25/0.75 quantiles, and 0.1/0.9 quantiles respectively.

SI Reference:

Dellaert S., Super I., Visschedijk A., Denier van der Gon H.A.C.: High resolution scenarios of CO_2 and CO emissions. https://www.che-project.eu/sites/default/files/2019-05/CHE-D4-2-V1-0.pdf, 2019.

Lian, J., Lauvaux, T., Utard, H., Bréon, F.-M., Broquet, G., Ramonet, M., Laurent, O., Albarus, I., Chariot, M., Kotthaus, S., Haeffelin, M., Sanchez, O., Perrussel, O., Denier van der Gon, H. A., Dellaert, S. N. C., and Ciais, P.: Can we use atmospheric CO_2 measurements to verify emission trends reported by cities? Lessons from a 6-year atmospheric inversion over Paris, Atmos. Chem. Phys., 23, 8823–8835, https://doi.org/10.5194/acp-23-8823-2023, 2023.

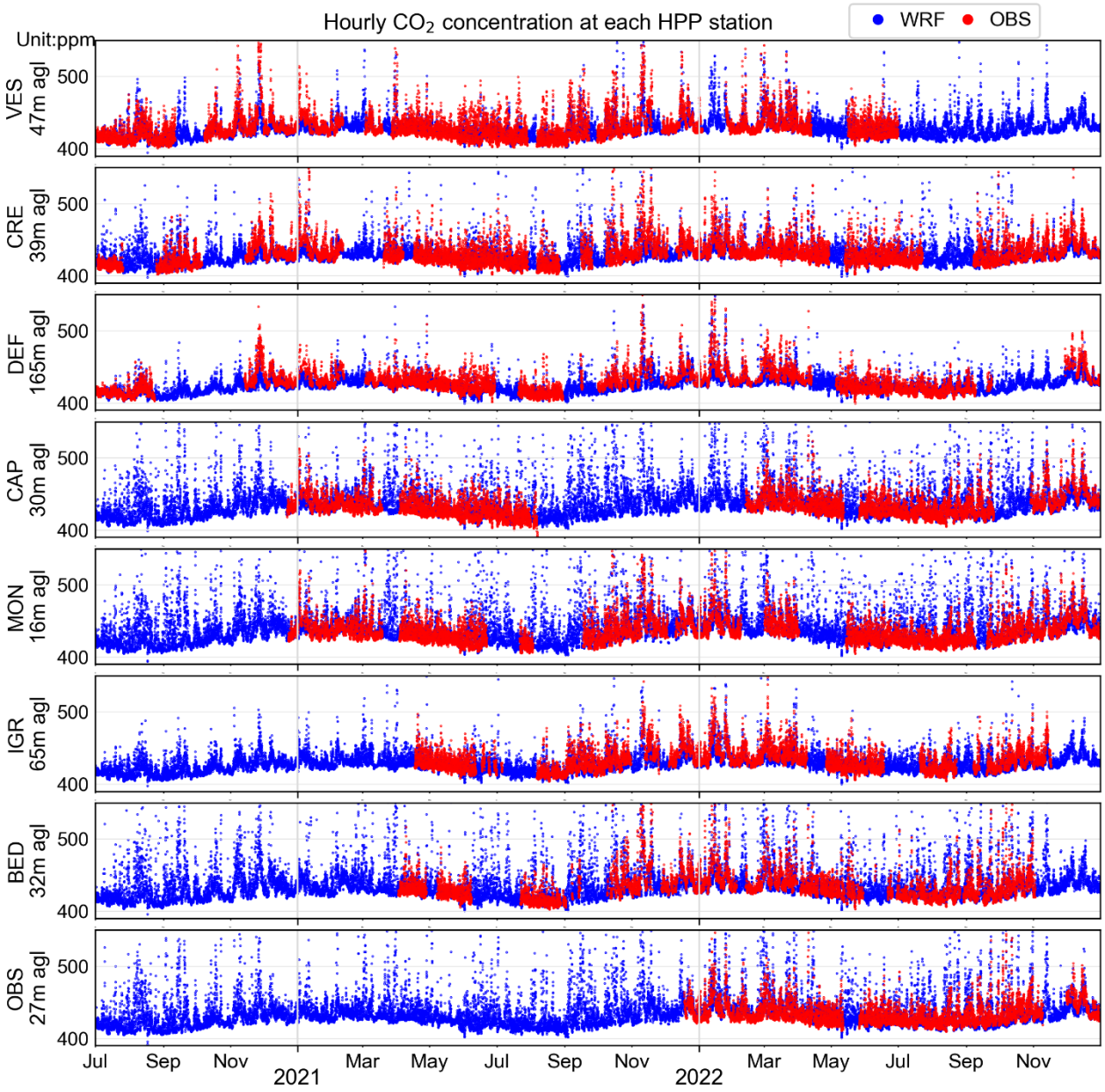

Figure S5. Time series of the modeled and observed hourly CO_2 concentration at each HPP station.

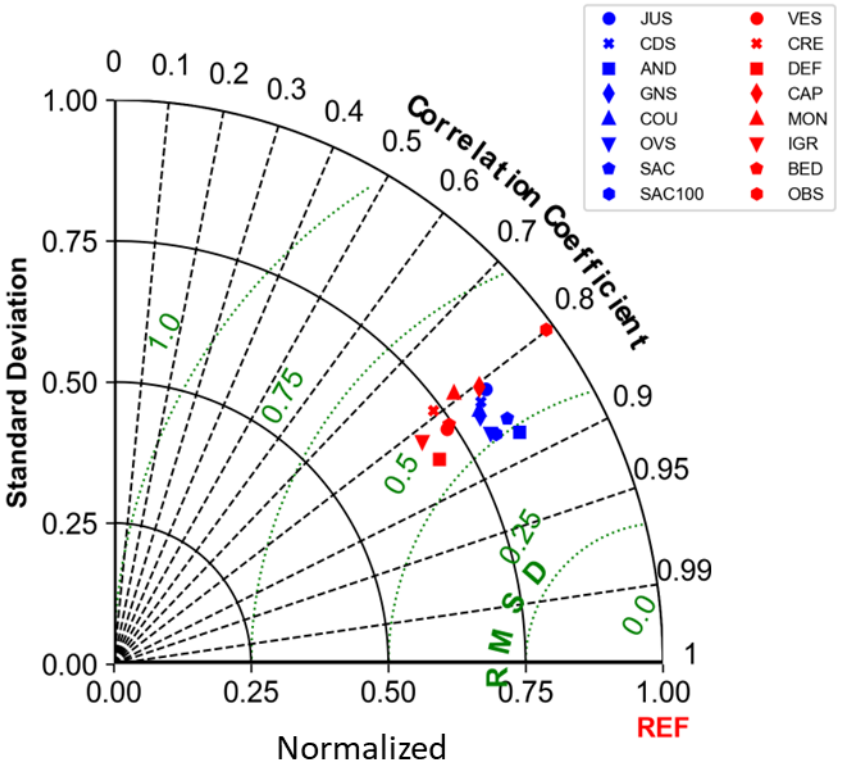

Figure S6. Comparisons of the observed and modeled hourly afternoon (12-17 UTC) CO_2 mole fractions at 7 CRDS and 8 HPP stations over the period of July 2020 to December 2022. The SAC station has two air inlets placed at 15 m and 100 m above ground level, respectively.

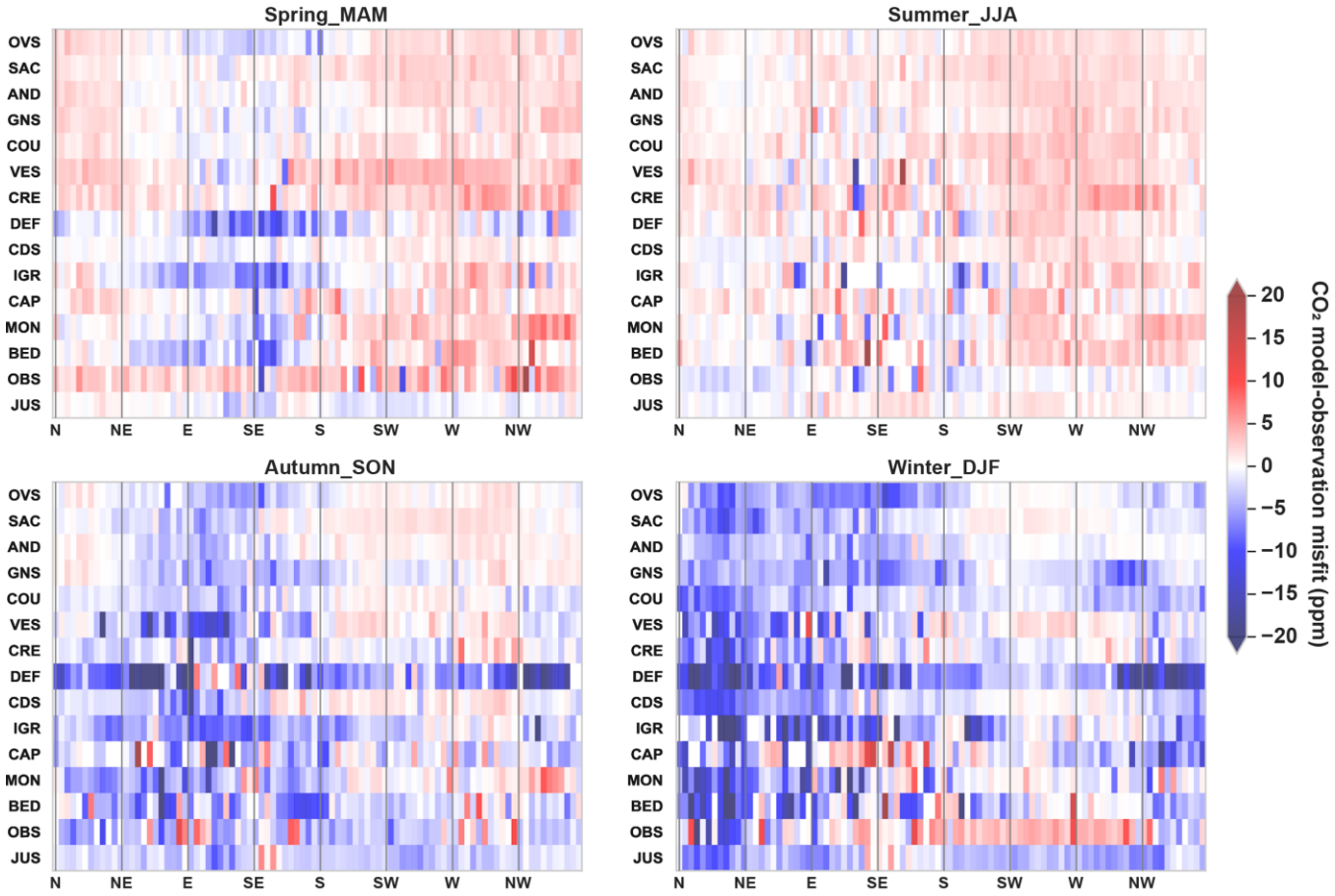

Figure S7. Model-observation misfits in hourly afternoon (12-17 UTC) CO_2 mole fractions, averaged accounting for wind direction for four seasons at 7 CRDS and 8 HPP stations over the period of July 2020 to December 2022. The stations are displayed in a bottom-to-top sequence, corresponding to their increasing distance from the JUS station.

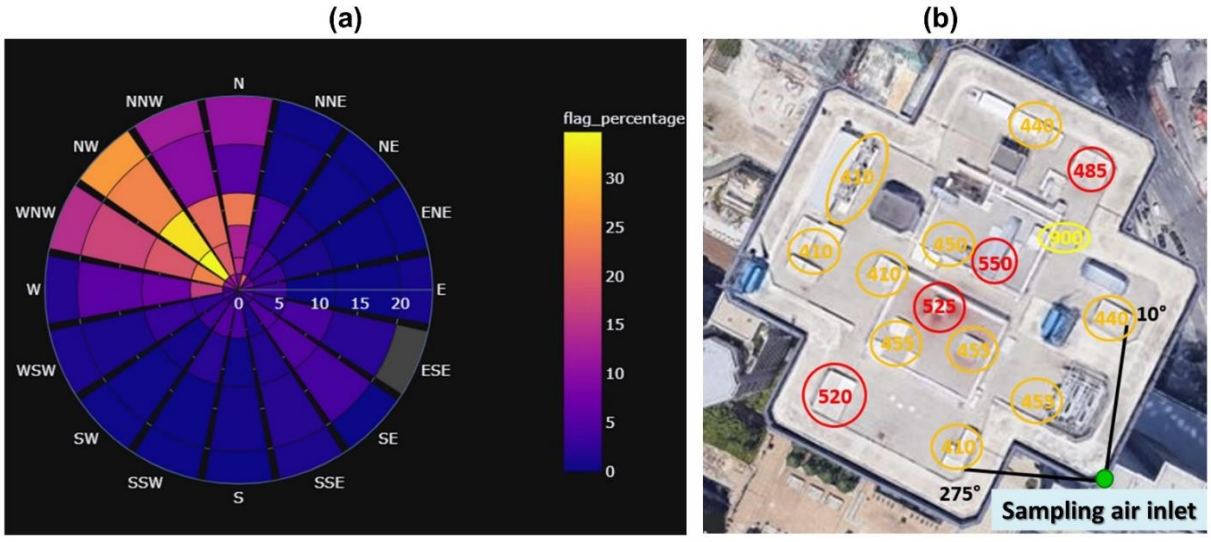

Figure S8. (a) Average spike percentage of observed CO_2 mole fractions as a function of wind speed and direction at DEF station from January to May 2021. (b) A photo of the rooftop at DEF station indicates potential local sources of contamination, primarily originating from the direction spanning 275° to 10°. Red circle: active and high-flow sources of contamination during the visit. Orange circle: potential sources of contamination not active or low flow during the visit. Yellow circle: a source of active contamination but

structurally at low flow (e.g., sanitary facilities). Green dot: the location of the sampling air inlet. The image in (b) was extracted from © google map.

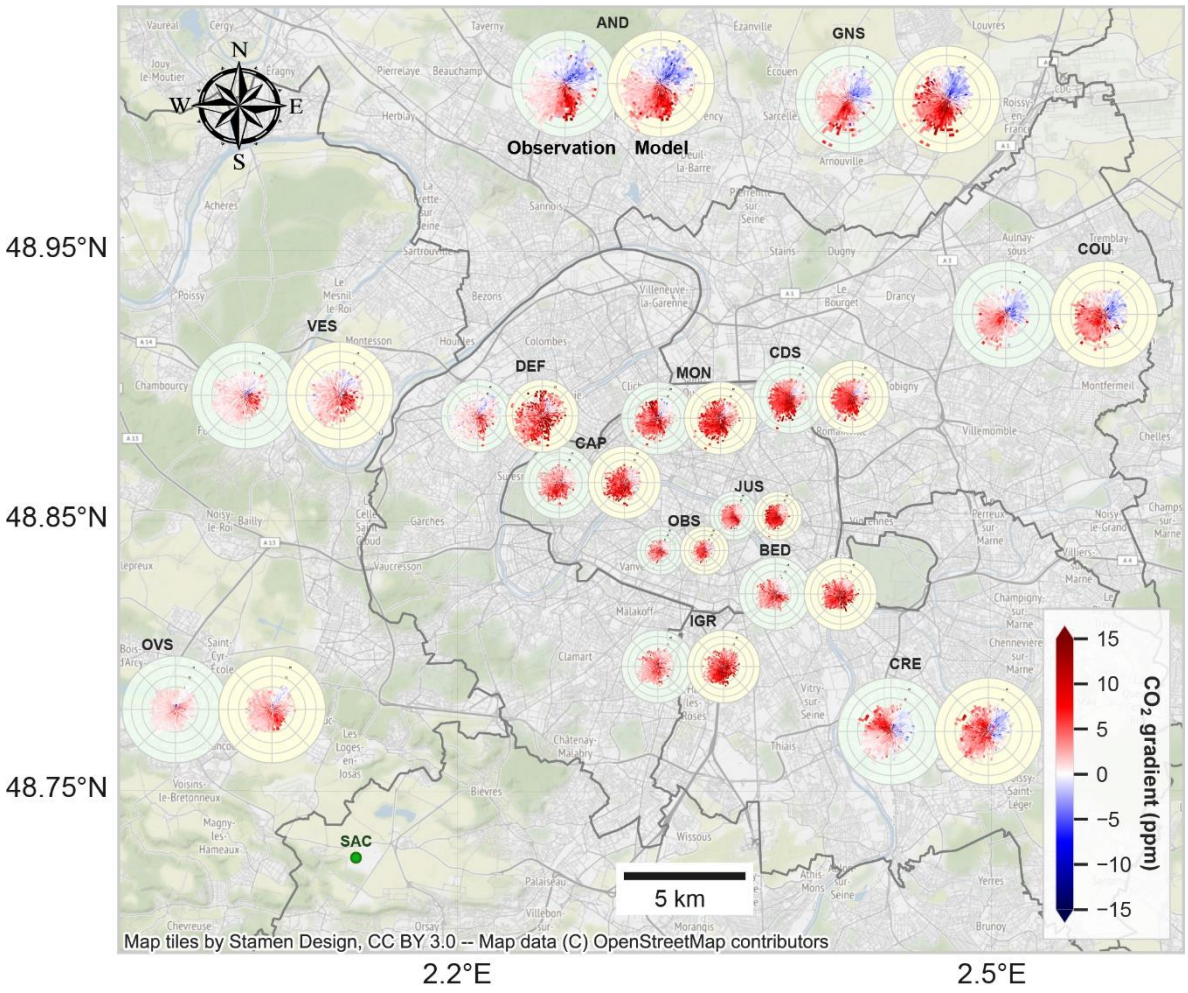

Figure S9. Observed (green panel) and modeled (yellow panel) CO_2 mole fraction differences between SAC and all the other stations, averaged accounting for wind speed and direction over the period of July 2020 to December 2022. Only the afternoon (12-17 UTC) data are used. The different sizes of the polar panels hold no specific meaning and are merely adjusted to avoid overlaps.

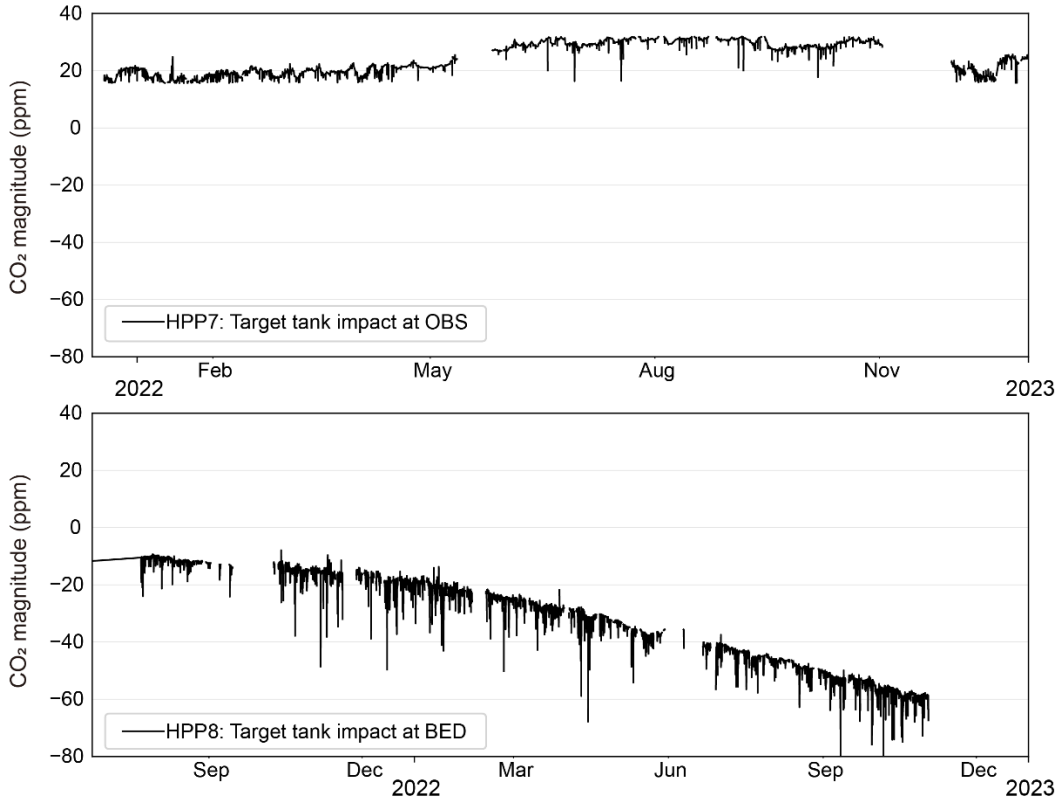

Figure S10. Evolution of the impact of the daily target gas injection in the calibration at two HPP sensors. It was calculated as the CO_2 differences before and after applying $CO_{2_{offset}}$ in Eq. (1).

Table S1. Ranges of acceptable values for critical physical parameters measured by the HPP instrument.

Parameter (unit)	Min value	Max value
H_2O (molar fraction)	0.2%	4%
Pump speed	0.1	0.95
Flowrate (L/min)	0.4	N/A
CO_2 (ppm)	350	700
Detector temperature (°C)	64.98	65.02
Main mirror temperature (°C)	66.90	67.10
Component block temperature (°C)	66.90	67.10
Microcontroller temperature (°C)	0	50